Crystal structure and physical properties of half-doped manganite nanocrystals of less than 100-nm size

Tapati Sarkar,[*] Barnali Ghosh, and A. K. Raychaudhuri[†]

DST Unit for NanoSciences, S. N. Bose National Center for Basic Sciences, Block JD, Sector III, Salt Lake, Kolkata 700 098, West Bengal, India

Tapan Chatterji

Science Division, Institut Laue-Langevin, BP 156, 38042, Grenoble, Cedex 9, France

In this paper we report the structural and property (magnetic and electrical transport) measurements of nanocrystals of half-doped $La_{0.5}Ca_{0.5}MnO_3$(LCMO) synthesized by chemical route, having particle size down to an average diameter of 15 nm. It was observed that the size reduction leads to change in crystal structure, and the room temperature structure is arrested so that the structure does not evolve on cooling unlike bulk samples. The structural change mainly affects the orthorhombic distortion of the lattice. By making comparison to observed crystal structure data under hydrostatic pressure, it is suggested that the change in the crystal structure of the nanocrystals occurs due to an effective hydrostatic pressure created by the surface pressure on size reduction. This not only changes the structure but also causes the room temperature structure to freeze. The size reduction also does not allow the long supercell modulation needed for the charge ordering, characteristic of this half-doped manganite, to set in. The magnetic and transport measurements also show that the charge ordering (CO) does not occur when the size is reduced below a critical size. Instead, the nanocrystals show ferromagnetic ordering down to the lowest temperatures along with metallic-type conductivity. Our investigation establishes a structural basis for the destabilization of CO state observed in half-doped manganite nanocrystals.

I. INTRODUCTION

The doped perovskite oxide manganites (with ABO_3 structure) are fascinating because they can readily be tuned between different electronic phases by proper substitution of cations. The ground state of the manganites can have distinct phases [a ferromagnetic (FM) metal, a charge-ordered (CO) insulator or a paramagnetic polaron liquid] which are energetically close.[1] The manganites contain interactions of different types that are often of comparable strength.[2] As a result the ground state of the manganites can be of different types depending on which of the interactions win over. The tuning of the ground state can be done by factors such as the carrier density, magnetic field, pressure, and biaxial strain. Of particular importance for the present investigation is the charge and orbitally ordered state observed in half-doped manganites that have equal amounts of Mn^{3+} and Mn^{4+} ions. The half-doped manganites give rise to charge-ordered state associated with a real space ordering of 1:1 Mn^{3+}/Mn^{4+} species accompanying a structural change.[3] Charge and orbitally ordered insulating state (COI) occurs in many half doped manganites like $La_{0.5}Ca_{0.5}MnO_3$,[4] $Pr_{0.5}Ca_{0.5}MnO_3$,[5] $Pr_{0.5}Sr_{0.5}MnO_3$,[6] $Nd_{0.5}Ca_{0.5}MnO_3$,[7] $Nd_{0.5}Sr_{0.5}MnO_3$.[8]

In this paper we investigate systematically the crystal structure and physical properties of nanocrystals of a specific half-doped manganite, $La_{0.5}Ca_{0.5}MnO_3$, with size down to 15 nm and study how size reduction to the nanometer dimensions can lead to a tuning of the ground state in these materials. $La_{0.5}Ca_{0.5}MnO_3$ has a transition from a paramagnetic to a ferromagnetic state around 225 K, followed by the charge ordering transition at $T=155$ K.[9] An antiferromagnetic order accompanies the charge ordering transition. In particular, we study the crystal structure of these nanocrystals using Synchrotron x-ray to establish the role of structure in tuning the physical properties. In perovskite oxides in general, a specific ordered state is generally favored by a specific crystal structure. Thus, in these nanocrystals, the study of the role of crystal structure in stabilizing a specific ground state is of utmost significance.

The insulating CO state can be destabilized to a FM metallic phase by a number of external perturbations that include magnetic field,[10] doping, biaxial strain and pressure,[11] and in some cases even electric field.[12,13] In this work, we have investigated what happens to the structure and physical properties of $La_{0.5}Ca_{0.5}MnO_3$ when we bring down the sizes from bulk ($\sim$3.6 μm) to sizes as small as 15 nm, a change in size of more than 2 orders of magnitude. Earlier reports of studies on half-doped manganites were done with particle sizes which were much larger, and in some cases, in excess of 100 nm.[14–16] These studies have reported modification of the charge-ordered state in these systems. However, no analysis of the crystal structure using high resolution x-ray diffraction data (as has been done here) has been made. We show that analysis of the crystal structure using high resolution powder diffraction data helps us to understand some of the crucial factors that lead to destabilization of the COI state in these manganites below a certain critical size. In particular, we show that an equivalent hydrostatic pressure (arising from the surface pressure) can lock the room temperature structure and not allow it to evolve on cooling as is required for the CO to set in. This is a study of the structural evolution of nanoparticles of manganites using high resolution diffrac-

tion techniques. A preliminary report of the structural data has been made recently by us.[17]

II. EXPERIMENT

We have adopted a polymeric (polyol) precursor route to synthesize $La_{0.5}Ca_{0.5}MnO_3$(LCMO) nanocrystals with sizes down to 15 nm. This method allows synthesis at a significantly lower sintering temperature compared to the conventional solid state procedure. In this technique the polymer (ethylene glycol in our case) helps in forming a close network of cations from the precursor solution, and assists the reaction, enabling phase formation at relatively low temperatures.[18] In a typical synthesis process, high purity (>99%)$(CH_3COO)_3La \cdot 1.5H_2O$, $Ca(CH_3CO_2)_2 \cdot H_2O$, and $(CH_3COO)_2Mn \cdot 4H_2O$ (procured from Sigma Aldrich[19]) were dissolved in the desired stoichiometric proportions in acetic acid and water. To this solution an appropriate amount of ethylene glycol (molecular weight=62.07 gm/mol) was added and heated until the sol was formed. The gel was dried overnight at ≈ 150 °C. Pyrolysis was done at 350 °C and 450 °C followed by a sintering at ≈ 650 °C to obtain the desired chemical phase. The water-ethylene glycol ratio, heat treatment employed during gelling, pyrolization, and calcination were found to influence the particle size of the final product. We optimized these process parameters to obtain phase pure LCMO nanocrystals with a particle size of ~ 15 nm [as established from x-ray diffraction (XRD) results, using Williamson Hall plot[20] and transmission electron microscopy (TEM) images]. If the experiments can be carried out without pellet formation such as the synchrotron x-ray studies, the nanocrystals with ~ 15 nm diameter can be used. We used pellets of the nanocrystals both for transport and magnetic measurements. These nanocrystals have been used for making samples of larger size by heat treatment. The pellets were sintered at different temperatures varying from 650 °C to 1300 °C and for varying time periods (5–30 h). The sintering at different temperatures and times leads to particle growths to different sizes making it possible to grow grain sizes as large as 3.6 μm or more. This ensures that the particles with different sizes have the same chemical stoichiometry since they have been prepared from the same batch of starting nanocrystals. All the synthesized samples were characterized using powder XRD using Cu $K\alpha$ radiation at room temperature to establish the purity of the chemical phases. The stoichiometry of the nanopowder was also checked independently by a quantitative analysis using inductively coupled plasma atomic emission spectroscopy (ICPAES). The pellets were also checked for oxygen stoichiometry using iodometric titration. Microstructural characterization of the pellets was done using field emission gun-scanning electron microscopy (FEG-SEM) including energy dispersive x-ray analysis (EDAX) and transmission electron microscopy (TEM).

The magnetic measurements have been carried out using a Quantum Design superconducting quantum interference device (SQUID) magnetometer[21] and also a homemade low field ac susceptibility bridge working at 33.33 Hz. The resistivity measurements were done using standard dc four-probe

TABLE I. Annealing conditions, particle size, and cell volume of the LCMO samples.

Sample ID	Annealing temperature (°C)	Annealing time (hrs)	Particle size (r) (nm)	Cell volume ($Å^3$)
A	650	5	15	221.0
B	750	10	43	221.1
C	850	10	141	222.5
D	950	10	378	224.6
E	1100	30	600	224.6
F	1300	2	3660	224.7

technique in the temperature range 4.2 to 300 K in a closed cycle refrigerator.[22] Magnetoresistance measurements were carried out in the temperature range 4.2 to 300 K under a field of 10 T using a bath type cryostat.

High resolution powder diffraction data were obtained at the European Synchrotron Radiation Facility, Grenoble, France using the BM-01B beamline and a wavelength of 0.375 Å, over the temperature range 5–300 K. The samples were in powder form and were kept in a borosilicate capillary. The calibration was done using standard Si samples. To extract the lattice parameters and study the structural evolution of the samples as a function of temperature, we used nearly 5000–6000 points/scan using six detectors. The Rietveld analysis of the lattice structure was done using the FullProf Suite software.[23]

III. RESULTS

A. Characterization: structure and stoichiometry

We synthesized six different samples having particle size ranging from 15 to 3660 nm by pelletizing the as-prepared powder and subjecting them to different annealing conditions as described before (see Table I). The XRD data were used to check that the samples prepared were of pure phase and to estimate the average particle size for the samples with lower particle size (see Table I). For larger particle size samples, the sizes were estimated from FEG-SEM images. The resolution of the FEG-SEM is 2 nm at the beam voltage used (5 kV). In the region of overlap, there is good agreement between the average size determined by the FEG-SEM and the XRD. Table I also shows the unit cell volumes of the nanocrystals as obtained from the x-ray data taken at room temperature. (Analysis of the powder diffraction data are given in a separate subsection below).

In Fig. 1 we show the high resolution transmission electron microscopy (HRTEM) images taken on nanocrystals of size ~ 15 nm. The inset shows the electron diffraction pattern, which confirms the single crystalline nature of the nanoparticles. The indexing of the points in the diffraction pattern was done following orthorhombic symmetry. The lattice planes have been indexed. The value of d [(111) planes] as obtained from the HRTEM images is ~ 0.345 nm. This is quite close to the value obtained from the XRD (~ 0.343 nm) data.
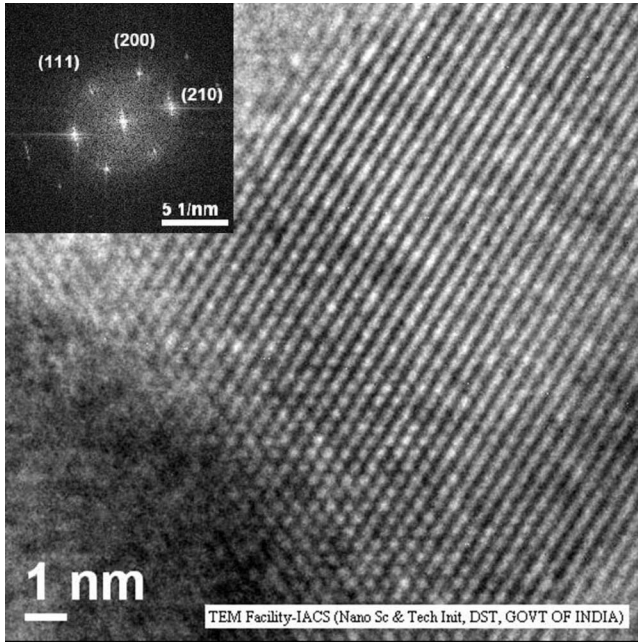
FIG. 1. HRTEM data of LCMO crystal of size 15 nm. The lattice parameter obtained is ~0.345 nm. The inset shows a typical diffraction pattern from a nanocrystal. The indexing has been done using orthorhombic symmetry.

The charge ordering phenomenon observed in $La_{1-x}Ca_xMnO_3$ (Ref. [1]) occurs at half doping with the carrier concentration $x \approx 0.5$. We have taken special care that the samples used have proper stoichiometry and hence the proper carrier concentration. Since we made all the samples starting from the same batch of nanoparticles (with size ~15 nm), they all have the same stoichiometry and the same carrier concentration irrespective of the size. We checked the stoichiometry using ICPAES. The particular batch of samples on which we report the data here yielded a La:Ca:Mn ratio of 0.507:0.495:1. We have checked that our synthesis method maintains a reproducible and good stoichiometry from batch to batch. The control of proper stoichiometry among the samples with different sizes allows us to be conclusive that any change of physical property arises only because of a reduction in the size. In addition, we have also checked the stoichiometry on the microstructural level from EDAX measurement done on each pellet at different points over a range of ~1 μm using the FEG-SEM. The spectral resolution was ≈10 nm. We find that the composition remained the same (the ratio La:Ca varies between 1.02 ± 0.04 throughout the scanned range in the samples used). We also checked the oxygen stoichiometry of the pellets by iodometric titration. All the pellets had some oxygen deficiency ($La_{0.5}Ca_{0.5}MnO_{3-\epsilon}$) with ϵ positive. $\epsilon \approx 0.021$ for the pellet with the smallest particle size, and it increases somewhat for the bulk sample. Thus the particles with smaller particle size have better oxygen stoichiometry.

B. Crystal structure analysis

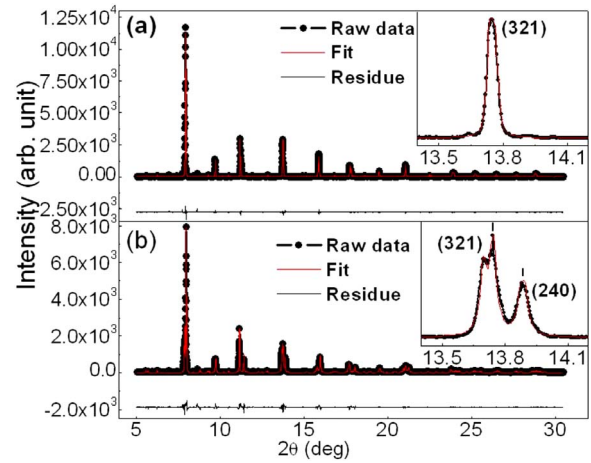In Figs. 2 and 3 we show the diffraction data taken at 5 K

FIG. 2. (Color online) XRD patterns (along with the fits) of the bulk sample (average particle size ~3.6 μm) taken at (a) 300 K and (b) 5 K. Insets show the expanded regions between $2\theta=13.4°$ and 14.2°. In the inset for 5 K, the positions of the peaks are shown by ticks.

and 300 K for the "bulk" (powder with grain size ≈3.6 μm) and the nanocrystal (average diameter ≈15 nm), respectively. In the same plots we also show the fits with the residues for both samples (details of the fitting are discussed later on). For the bulk sample, the data taken at 300 K are very different from that taken at the lowest temperature of 5 K. At 5 K we very clearly see splitting of reflections and the appearance of extra weak reflections in the x-ray diffraction patterns, which are the signatures of small structural distortions occurring due to charge and orbital ordering. The appearance of these extra Bragg reflections have been associated with the presence of J-T distortion of the $Mn^{+3}O_6$ octahedra.[4] On the other hand, the diffraction pattern of the nanocrystal remains virtually unchanged throughout the temperature region scanned, i.e., the scan taken at 300 K is virtually the same as that taken at 5 K with no appearance of
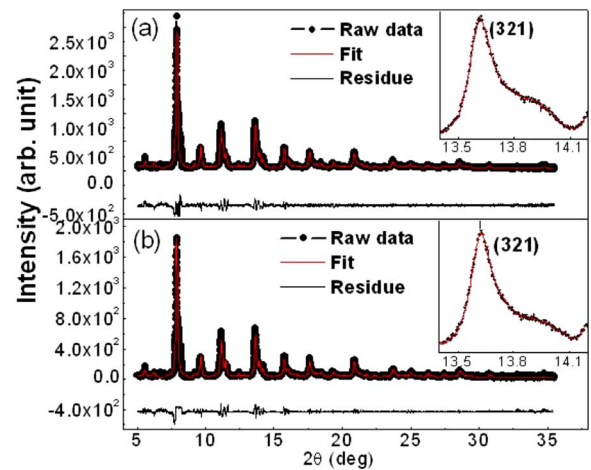

FIG. 3. (Color online). XRD patterns (along with the fits) of the nanoparticle sample (average particle size ~15 nm) taken at (a) 300 K and (b) 5 K. Insets show the expanded regions between $2\theta=13.4°$ and 14.2°. In the inset for 5 K, the positions of the peaks are shown by ticks.
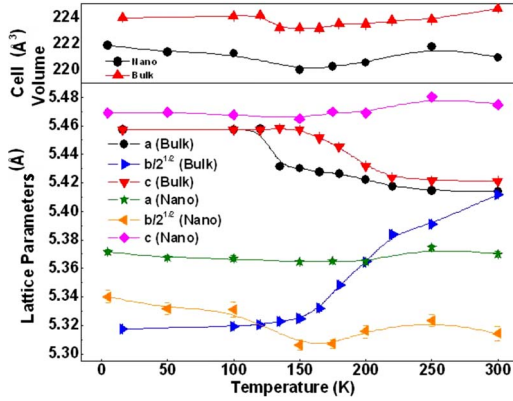
FIG. 4. (Color online). Variation of lattice parameters and cell volume for bulk and nano-LCMO (average particle size ∼15 nm). Error bars, where not visible, are smaller than the symbols.

FIG. 5. (Color online). Variation of the orthorhombic strains for bulk and nano-LCMO (average particle size ∼15 nm). Error bars that are not visible are smaller than the symbols.

any extra peaks. This itself is the first indication that the structure of the nanocrystals fails to evolve as it should on lowering the temperature if charge and orbital ordering have to set in.

The high resolution diffraction data of the samples were analyzed using a profile fitting technique to obtain the crystal structure parameters. The x-ray line profiles were modeled using a pseudo-Voigt profile shape function. We show some representative fits along with the residues for both samples in Figs. 2 and 3. This analysis was done to quantitatively study the changes in the basic structure of $La_{0.5}Ca_{0.5}MnO_3$ as a result of the size reduction. One obvious difference arising due to size reduction is in the shape of the peaks, the peaks in the nanoparticle sample being more broad and asymmetric than those in the bulk sample. This difference in the line shape can be taken care of through the asymmetry parameter[23] β. For the bulk sample, $\beta_{bulk}=0.08$ and that for the nanocrystals, $\beta_{nano}=0.61$ at $T=300$ K. With cooling, β increases for both samples ($\beta_{bulk}=0.21$ and $\beta_{nano}=0.66$ at $T=5$ K), but the increase is much more in the bulk sample than that in the nanoparticle sample. Here we note that we did the analysis using the higher symmetry space group *Pnma* at all temperatures. Below the charge ordering temperature the structure of the bulk sample undergoes an orthorhombic to monoclinic transition, which will reduce the crystallographic symmetry from *Pnma* to $P2_1/m$.[4] However, here we report the refined values of the lattice parameters only (and not the atomic positions), and so the reported values are quite reliable. In fact, fitting the low temperature data using the space group $P2_1/m$ changes the refined values of the lattice parameters by only ∼0.0016% (these values are not reported here). This change is lower than the percent error of 0.03%. So effectively the values of the lattice parameters become independent of whether we use the space group *Pnma* or $P2_1/m$.

In Fig. 4 we show the temperature evolution of the lattice parameters for the bulk, as well as the nanoparticle sample with the smallest average particle size. In the same graph we also show the dependence of the unit cell volume. The variations of the lattice constants with temperature are sharply different in the nanocrystals and the bulk sample. For the nanocrystals, throughout the temperature range studied, all
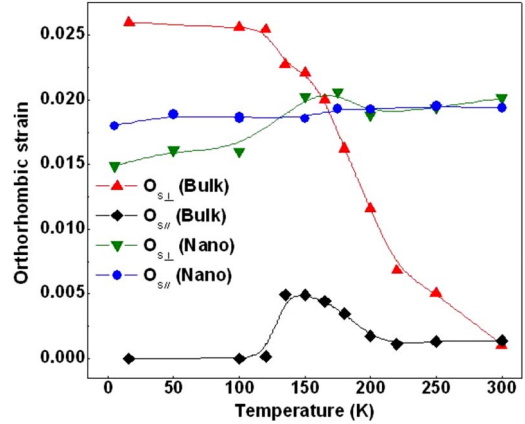
the lattice constants remain essentially unchanged. There are no systematic changes in the lattice constants on cooling. At room temperature, the nanocrystals have the *a* axis smaller by ≈1% compared to the bulk. The compaction in the *b* axis is ≈2% while the *c* axis expands by ≈1%. At the lowest temperature (5 K) due to the large changes in the lattice constants of the bulk sample, the lattice constants *a* and *c* become comparable in the bulk samples while the *b* axis becomes smaller. The absence of any temperature variation of the lattice constants of the nanocrystals shows that the room temperature structure is indeed arrested in the nanocrystals. This arrest of the room temperature structure in the nanocrystals thus prevents the evolution of the low temperature charge-ordered phase.

The lattice parameters of bulk LCMO (unlike those of the nanocrystals) display large changes in the region $T_{CO}<T<T_C$. At 300 K, the three axes have similar size. With cooling, the *b* axis decreases drastically, and the *a* and *c* axes increase correspondingly. The changes become more pronounced below 200 K and they become nearly temperature independent for $T<T_{CO}$. These changes in the lattice parameters are associated with the structural changes, which occur as the bulk sample undergoes the charge ordering transition and are characteristic of bulk LCMO. The observed changes in the lattice constants for the bulk sample match well with the data published on bulk samples before.[4]

One important quantity that changes due to the size reduction are the orthorhombic strains ($O_{S_\parallel}$ and $O_{S_\perp}$).[17] These are shown for the two samples in Fig. 5. The orthorhombic strain $O_{S_\parallel}$ gives the strain in the *ac* plane and is defined as $O_{S_\parallel}=2(c-a)/(c+a)$, while $O_{S_\perp}$ gives the strain along the *b* axis with respect to the *ac* plane and is defined as $O_{S_\perp}=2(a+c-b\sqrt{2})/(a+c+b\sqrt{2})$. In the bulk sample, the largest change occurs in $O_{S_\perp}$, which increases substantially as the sample is cooled and reaches a saturation value of ≈0.026 below the charge ordering temperature T_{CO}. On the other hand, $O_{S_\parallel}$ shows a rather small value over the whole temperature range while showing a small enhancement in the temperature range where the CO sets in but again becoming negligible for $T<T_{CO}$. In the nanocrystal, since the lattice constants are
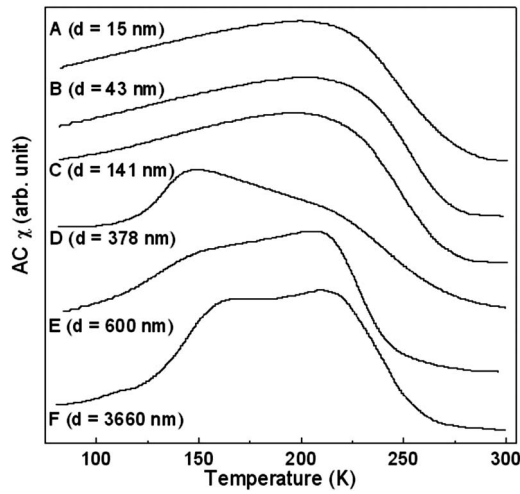
FIG. 6. AC susceptibility vs temperature for the LCMO samples having different particle sizes.

FIG. 7. Variation of T_{CO} and FM % as a function of particle size.

more or less temperature independent, both $O_{S_{\parallel}}$ and $O_{S_{\perp}}$ are temperature independent over the whole temperature range, and they have similar magnitudes. The orthorhombic strains that rapidly change in bulk samples at $T \approx T_{CO}$ is completely absent in the nanocrystals, and as stated before the $O_{S_{\perp}}$, as well as $O_{S_{\parallel}}$, remain locked at their room temperature values.

The lattice parameters in the nanoparticle sample are in a sequence $b/\sqrt{2} < a < c$, i.e., $a < c$. In some half-doped manganites, the opposite trend has been reported, i.e., $c < a$.[24] However, in this case, we can rule out the possibility that $c < a$, for the reason that the error in the refined values of the lattice parameters is much less than the difference between a and c. The errors in the values of a and c are of the order of 0.001, whereas the difference between a and c is of the order of 0.01. So in this case a is definitely less than c. Here, we would also like to note that even in the bulk sample, c is always greater than a. In the nanoparticle sample, this difference further increases thereby increasing the orthorhombic strain $O_{S_{\parallel}}$.

C. Magnetic measurements

The structural changes that are observed in the nanocrystals are accompanied by distinct changes in the magnetic properties of the samples. Charge ordering in LCMO system is accompanied by spin ordering. In bulk LCMO, it has been reported that the spin ordering is an antiferromagnetic transition to CE-type ordering with the Néel temperature $T_N \approx 155$ K. This transition shows up as a drop in the susceptibility following the high temperature transition from paramagnetic to ferromagnetic state at $T_C \approx 225$ K. Figure 6 shows the temperature dependence of the low field ac susceptibilities (taken by mutual inductance bridge) of LCMO samples of different sizes ranging from the highest (3660 nm) to the lowest (15 nm) particle sizes. All the samples undergo a transition from paramagnetic to ferromagnetic state at around 230–250 K, where the T_C is identified by the inflection points in the dM/dT versus T plots. Interestingly, the T_C determined by the low field ac susceptibility increases
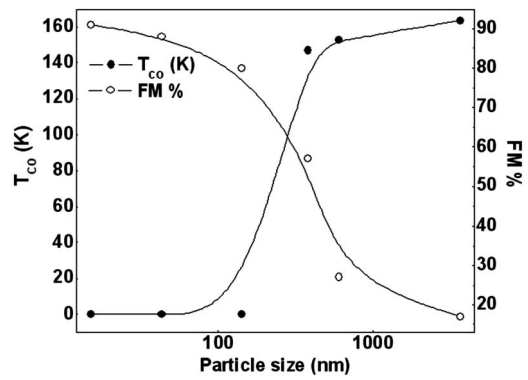
with size reduction, signifying strengthening of the ferromagnetic interaction on size reduction. As the temperature is decreased further, the susceptibility of the bulk sample (average particle size ≈ 3660 nm) starts to decrease at $T \approx 150$ K, and the transition is mostly over by $T \approx 135$ K. This is the signature of the onset of the antiferromagnetic (AFM) order accompanying the CO, as has been seen earlier in bulk samples.[9] Such a drop in the susceptibility at lower temperatures is absent in nanocrystals of size ≤ 150 nm. This would imply that the AFM order that accompanies the CO is absent in nanocrystals with sizes smaller than 150 nm. In Fig. 7 we plot T_{CO} and the ferromagnetic fraction as determined by the magnetization (magnetization shown later on) as a function of particle size. It can be seen clearly that both T_{CO}, as well as the FM fraction, show a sharp transition when the particle size goes below 150 nm. The size reduction thus inhibits formation of the CO ground state, and the ferromagnetic state is stabilized.

The magnetization data support the observation as made in the ac susceptibility. The magnetization data taken on the "bulk" sample, as well as on the nanocrystals, are shown in Fig. 8 at two fields (0.01 T and 5 T). The bulk sample (lower panel) shows the transition from paramagnetic to ferromagnetic state, where the magnetization rises, and then on further cooling as the AFM order sets in, it falls as seen in the ac
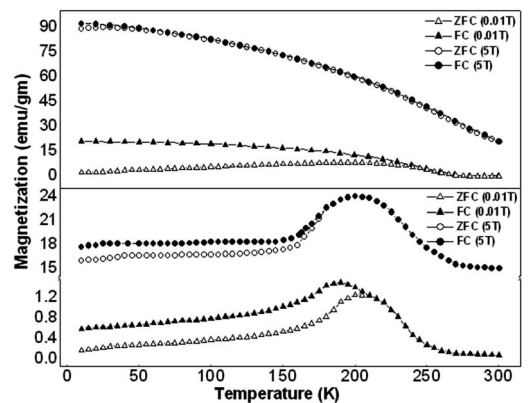

FIG. 8. Magnetization vs temperature for the nanoparticle sample (upper panel) and bulk sample (lower panel) of LCMO under a magnetizing field of 0.01 T and 5 T.
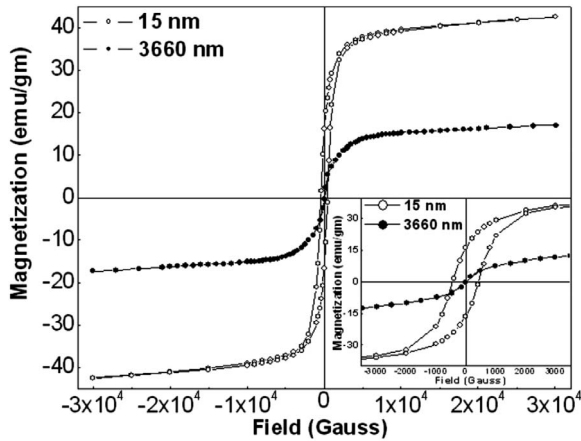
FIG. 9. Magnetization vs field for bulk and nano-LCMO at a temperature of 5 K. The inset shows an expanded portion of the MH loop near the origin.
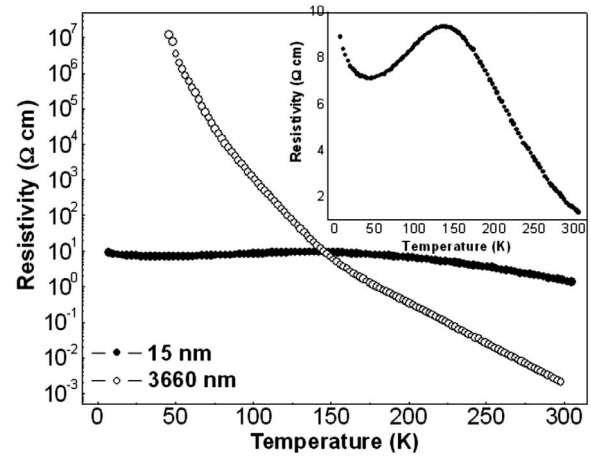

FIG. 10. Resistivity vs temperature for LCMO (15nm) and bulk LCMO. Inset shows the resistivity of the nanoparticle sample on an extended scale.

susceptibility data. At lower field (≈ 0.01 T) there is a clear separation of the zero field cooled (ZFC) and field cooled (FC) data, which occurs close to the temperature where the magnetization shows a peak. This is a signature of irreversibility that may arise due to remanent spin disorder in the sample. The magnetic moment at 10 K at 5 T field is ≈ 0.6 $\mu_B/\mathrm{f.u.}$. This is substantially less than that expected from fully ferromagnetically aligned moments. The AFM order that sets in along with the CO transition is thus stable down to the lowest temperature in the bulk sample in a field of 5 T. In contrast to the bulk sample, the nanocrystals do not show any magnetic transition below the transition from paramagnetic to ferromagnetic state. The magnetization of the nanocrystals at $H = 5$ T rises monotonically (for both FC and ZFC cases) and approaches toward saturation at the lowest temperature. The magnetization at 10 K is ~ 3.18 $\mu_B/\mathrm{f.u.}$ This is $\sim 91\%$ of M_S (=3.5 $\mu_B/\mathrm{f.u.}$, calculated assuming full ferromagnetic alignment of the spins for La$_{0.5}$Ca$_{0.5}$MnO$_3$). For the intermediate samples data are not shown to avoid repetition. The saturation moment determined from the magnetization has been shown in Fig. 7 before.

A plot of inverse susceptibility ($1/\chi$) vs temperature for the samples in the paramagnetic region show a Curie Weiss law $[\chi = C/(T - \theta)]$, where C is the Curie constant, and θ is the Weiss temperature. The Curie temperatures in all the samples are ferromagnetic. From the Curie constant C, we could calculate the effective magnetic moment μ_{eff}. For the 3660 nm bulk sample $\mu_{\mathrm{eff}} \approx 4.14$ μ_B and for the 15 nm nanocrystal $\mu_{\mathrm{eff}} \approx 4.36$ μ_B. This establishes that the paramagnetic state of LCMO is not much affected by the particle size. The main effect arises on cooling below the first transition from paramagnetic to ferromagnetic state and the subsequent presence or absence of the antiferromagnetic transition. The magnetic moment enhancement at low temperatures in the nanocrystals distinguishes the two ground states seen in the bulk sample and the nanocrystals.

In Fig. 9 we show the magnetization (M) vs magnetic field (H) curves for the bulk (average particle size ~ 3660 nm) and nanoparticle (average particle size

~ 15 nm) samples taken at 5 K. Compared to the bulk sample, which shows no hysteresis in the MH loop, the nanoparticle sample shows a considerable hysteresis with a coercive field of ~ 0.05 T and a remanence magnetization of ~ 16 emu/gm (see inset of Fig. 9). In contrast there is no remanence or coercive field in the larger size particles (bulk sample).

The magnetization data show that the nanocrystals retain their ferromagnetic state as they are cooled to lower temperatures unlike the bulk sample that shows the antiferromagnetic transition. The data also show that there is a significant enhancement of the ferromagnetic moment in the nanocrystals.

D. Electrical transport and magnetoresistance

Electrical resistivity provides strong evidence for the charge and orbital ordering transition when the sample enters an insulating state on charge ordering. Often the charge ordering transition is reflected as a change in slope in the resistivity plot. CO state also shows a very strong magnetoresistance in some of the manganites as the insulating state is destabilized by an applied field, which leads to creation of ferromagnetic metallic state. In the present investigation, particularly for the nanocrystals, the particle size being small the transport experiments have interference from the presence of a large contribution of grain boundaries in the electrical, as well as magnetotransport behavior. However, we show below that despite the interference, one can distinguish the electrical and the magnetotransport behaviors in samples that have large grains (~ 3660 nm) and those which have nanocrystals (≈ 15 nm).

In Fig. 10 we show the behavior of the resistivities of the two samples [3660 nm (bulk) and 15 nm samples] as a function of temperature from 4.2 to 300 K. The data are shown in the log scale. In nanoparticles, the resistivity at room temperature is about 3 orders higher than that of the bulk sample. In this temperature range both the samples are in a charge and orbitally disordered paramagnetic state. The
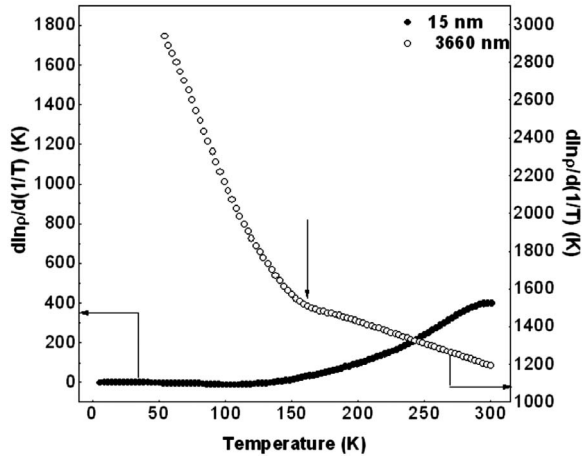
FIG. 11. $d \ln \rho / d(1/T)$ vs temperature for LCMO (15 nm) and bulk LCMO.

FIG. 12. MR as a function of temperature for LCMO (15 nm) and bulk LCMO

higher resistance of the sample with nanocrystals reflects the enhanced grain boundary contribution. In the bulk sample, however, the resistivity rises rapidly as the sample is cooled through the CO transition, and at 50 K the resistivity in the bulk sample becomes more than 6 orders higher than that in the nanoparticles. The bulk sample shows an insulating behavior throughout the temperature range. The charge ordering transition is reflected as a change in slope in the resistivity plot in the bulk sample. This can be seen in Fig. 11 where we plot $d \ln \rho / d(1/T)$, which gives the transport activation energy at temperature T. For the bulk sample we find a clear change in slope (at $T \approx 150$ K) showing hardening of the transport gap on cooling through the CO temperature.

The transport data of the sample with 15 nm nanocrystals are also shown in Fig. 10. In contrast to the sample with 3660 nm particle size, these samples show much less sensitivity to temperature, and the resistivity does not vary much on cooling (within one order). The resistivity of this sample shows a shallow peak at $T_P \sim 160$ K (seen more clearly in the inset of Fig. 10). In conventional ferromagnetic manganite La$_{1-x}$Ca$_x$MnO$_3$ with $x \approx 0.3$, a metal-insulator transition occurs close to the ferromagnetic transition where the material shows transition from a polaronic insulating paramagnetic state to a ferromagnetic metallic state. Thus, a peak in the resistivity occurs close to T_C. For this sample the magnetic data show a $T_C \sim 225$ K. Thus, T_P is significantly lower than T_C. Such a behavior is expected when the material is not a homogeneous metallic phase, but it is percolative in nature because of a large number of grain boundaries or the presence of an insulating phase coexisting with the metallic phase. The resistance again starts to rise below 55 K, presumably due to predominant contribution of the insulating grain boundaries to the overall current transport. Such behavior has been seen in nanostructured ferromagnetic films of manganites.[25] The plot of $d \ln \rho / d(1/T)$ for the nanoparticle sample (Fig. 11) shows that unlike the bulk sample, there is no clear change at around 150 K, which one would expect if the system showed a CO transition. If anything, it shows a gradual decrease in slope. An analysis of the resistivity data shows that there is indeed a signature of suppression of the CO insulating phase in the nanoparticles, and the phase that
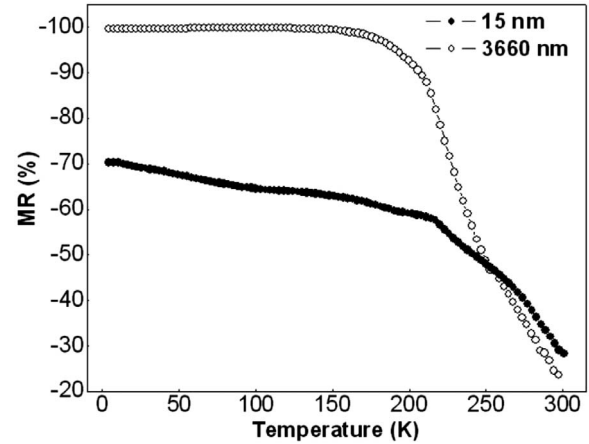
forms is metallic in nature although it is a percolative type of bad metal because of the existence of a large number of grain boundaries or even a coexisting insulating phase.

The magnetoresistance (MR) {defined as $100[\rho(H) - \rho(0)]/\rho(0)$ (with $H = 10$ T)} for both the bulk (average particle size ~ 3660 nm) and nanoparticle sample (average particle size ~ 15 nm) are plotted as a function of temperature in Fig. 12. In both samples the MR is negative although the value, as well as the temperature dependence, is qualitatively different. The insulating state of the CO bulk sample is completely suppressed on application of 10 T magnetic field. This is due to magnetic field-induced destabilization of the CO state that has been seen in many CO systems. The MR at the lowest temperature is nearly 100% for the bulk sample for $T < 100$ K. In contrast, in the nanocrystal sample, the MR increases slowly as it is cooled and reaches the limiting value of $\sim 70\%$. The behavior of the MR in the nanocrystal is similar to that seen in nanostructured films of ferromagnetic manganites,[26,27] which arises predominantly due to the grain boundary contributions. The MR data of the two samples also corroborate with the earlier observation about the predominant phases present in the two samples.

IV. DISCUSSION

In this paper, we have studied how the crystal structure and the physical properties of La$_{0.5}$Ca$_{0.5}$MnO$_3$ evolve on reducing the particle size by more than 2 orders of magnitude. We find a drastic change in the structure of the system on size reduction. The magnetic, as well as magnetotransport behavior of the nanocrystals, also shows qualitative changes in the nanocrystals. In the nanocrystals the CO state does not develop, and the ferromagnetic order is stable down to lowest temperatures. At room temperature the nanocrystals are more distorted than the bulk sample, as is evidenced from the higher values of the orthorhombic strains at room temperature in the nanoparticle sample. However, this distortion is temperature insensitive as is clear from Figs. 4 and 5. These observations bring forward some questions: First, why the crystal structure of the nanoparticles is different and the

room temperature structure does not evolve with temperature unlike the bulk crystal, and second, what prevents the CO to develop on cooling and whether the structure has a role to play.

To explain this change in the structure on size reduction we make the proposition that the surface pressure makes the nanocrystals behave as material under high hydrostatic pressure which not only changes the structure, but also "locks" the room temperature structure. Below, we justify this proposition. If we assume our particles to be spherical in shape, then the surface pressure acting on the particles is given by $P_s = 2S/d$, where d is the diameter of the particle, and S is the surface tension. The exact value of S for manganites is not known, but for perovskite oxide titanates, $S \approx 50$ N/m.[28] Putting in the values, we find that a pressure of $P_s \approx 6$ GPa acts on the sample with average particle size ~ 15 nm. It is clear that for particles of larger size (≥ 100 nm) the surface pressure will be very small (≤ 1 GPa) and thus will be of no consequence. The hydrostatic pressure will lead to reduction in cell volume as has been observed. From the observed cell volume change ($\sim 1.7\%$) using the typical bulk modulus of manganites as ~ 150 GPa, we find that a hydrostatic pressure of ~ 6 GPa will lead to a reduction in cell volume of $\sim 4\%$, which is similar to but larger than the observed reduction. This simple argument explains that the surface effect can indeed produce enough hydrostatic pressure to explain the change in the unit cell volume. Since the effect of surface pressure is to produce an effective hydrostatic pressure, it will be worthwhile to make connection with recent direct investigation of crystal structure under applied hydrostatic pressure as reported recently.[29] Our data for the nanoparticle sample (which we consider to be under an effective pressure of ~ 6 GPa) match very well with the crystal structure data of bulk sample measured under directly applied hydrostatic pressure of the same magnitude. Thus comparison to the hydrostatic pressure data establishes that the nanocrystal samples are under an effective hydrostatic pressure created by surface pressure due to its small size. It is this effective pressure that causes the crystal structure to deviate from the bulk structure.

The related issue is what causes the room temperature crystal structure of the nanocrystals not to evolve with temperature as the sample is cooled unlike the bulk sample. We suggest that the effective hydrostatic pressure created by the size reduction acts like a "clamp" that freezes-in the room temperature structure. The structural evolution on cooling in the bulk sample involves expansion of a and c axes and contraction of b axes. It is likely that the hydrostatic pressure prevents the lattice expansion. As a rough estimate using the $\sim 1.7\%$ unit cell compaction as a strain due to the effective hydrostatic pressure of 6 GPa, we find that the energy involved is ≈ 60 meV, which is larger than the thermal energy. This will justify why the effective hydrostatic pressure P_s will freeze-in the room temperature structure.

The effect of size reduction is to cause a change in the lattice structure. The onset of CO needs a particular type of crystal structure (or distortion) to support it. It is thus tempting to connect the absence of CO in nanocrystals to the structural factors. One reason can be that the particular type of orthorhombic distortion, where $O_{S_\perp}$ is substantially larger

than $O_{S_\parallel}$, is needed for the CO to set in, and this is absent in the nanocrystals where $O_{S_\perp} \approx O_{S_\parallel}$. This may prevent the CO to set in. Also, the development of CO needs creation of a modulated structure and a supercell as has been seen in bulk samples of $La_{0.5}Ca_{0.5}MnO_3$.[4] The propagation vector of the CO modulated structure is $(1/2 + \epsilon, 0, 0)$, where $\epsilon \approx 0.01$. This implies that the periodicity of the supercell is $\approx 200a \approx 106$ nm. Thus, if the particle size is less than ~ 100 nm, the supercell modulation needed for the CO cannot develop. In our case the size of the nanocrystals is more than seven times less than this value. It appears that the absence of a supercell modulation can be another cause why the CO does not set in in the nanocrystals.

It will be worthwhile to explore the other possible mechanisms, which might lead to the suppression of the charge ordered state, and investigate whether they have any relevance in our case. One of the likely mechanisms can be site or surface disorder. While disorder can most definitely lead to a destabilization of the charge ordered state, it is not clear why this should lead to an enhancement and strengthening of the ferromagnetic interaction as we observe in the nanocrystals. In fact, both site, as well as surface disorder, should lead to a decrease in the ferromagnetic T_C and the ferromagnetic moment.[30,31] In our samples, we find just the opposite trend, i.e., an enhancement in the ferromagnetic T_C, as well as an increase in the ferromagnetic moment, as the particle size is reduced. In fact, we note here that the nanocrystals do not have much spin disorder. The high field differential susceptibility ($\partial M / \partial H$), which can be taken as a measure of the spin disorder is the same in both the nanoparticles and the bulk samples ($\partial M / \partial H \approx 0.025$ emu/gm.k Gauss at 3 T). While disorder as seen in the grain boundary or grain surfaces appears to be an unlikely cause, one cannot rule out random local strain arising from inhomogeneous strain as a factor. This can act as a random field that can indeed destabilize the CO state. At present we cannot rule this out, and it may happen that the random field can act in tandem with the surface pressure arising from size reduction and lead to destabilization of the CO phase and creation of the FM order. It may be emphasized that the x-ray data show that the change occurs in the "bulk" of the nanocrystals and not in the surface.

At the end it may be pointed out that manganites in nanoscale are extremely interesting because it may be one of the few known systems where the metallic state (with ferromagnetic interaction) is stabilized by size reduction. In almost all the reported oxide systems the size reduction destabilizes the metallic state, and one obtains transition to an insulating state.[32] Manganites have competing interactions with almost equal strengths. The size tuning thus provides a subtle change in the balance between relative strengths leading to destabilization of one phase. This investigation establishes that the ground state property of manganites can be tuned by size reduction and also suggests that the tuning may actually occur due to change in structural parameters.

V. CONCLUSIONS

In summary, we have studied, in detail, the effect of size reduction on the crystal structure and physical properties of

$La_{0.5}Ca_{0.5}MnO_3$ nanocrystals, which were synthesized using the polymeric precursor route. The size was reduced down to an average size of 15 nm by using chemical methods. It was observed that the size reduction leads to change in crystal structure, and the room temperature structure is arrested so that structure does not evolve on cooling unlike bulk samples. The change in the structure was ascribed to an effective hydrostatic pressure created by surface pressure, which not only changes the structures but causes the room temperature structure to freeze. The size reduction does not allow the long supercell modulation needed for the CO to set in. The magnetic and transport measurements also show that the CO does not occur when the size is reduced below a critical size. The nanoparticle samples show enhanced ferromagnetic moment and metallic type conductivity. Our investigation establishes a structural basis for the destabilization of CO state in nanocrystals. Though the experiment has been carried out in the specific context of $La_{0.5}Ca_{0.5}MnO_3$, it is not unreasonable to expect similar behavior in other half-doped manganites. In fact the concept, that the surface pressure can create an effective hydrostatic pressure and that can act as a change agent may be applicable in other systems whose properties can change substantially with moderate hydrostatic pressure.

*tapatis@bose.res.in

†arup@bose res.in

[1] *Colossal Magnetoresistance, Charge Ordering and Related Properties of Manganese Oxides*, edited by C. N. R. Rao and B. Raveau (World Scientific, Singapore, 1998).

[2] John B. Goodenough, Phys. Rev. **100**, 564 (1955).

[3] C. N. R. Rao, Anthony Arulraj, A. K. Cheetham, and Bernard Raveau, J. Phys.: Condens. Matter **12**, R83 (2000).

[4] P. G. Radaelli, D. E. Cox, M. Marezio, and S. W. Cheong, Phys. Rev. B **55**, 3015 (1997).

[5] S. Mori, T. Katsufuji, N. Yamamoto, C. H. Chen, and S. W. Cheong, Phys. Rev. B **59**, 13573 (1999).

[6] R. Kajimoto, H. Yoshizawa, Y. Tomioka, and Y. Tokura, Phys. Rev. B **66**, 180402(R) (2002).

[7] T. Vogt, A. K. Cheetham, R. Mahendiran, A. K. Raychaudhuri, R. Mahesh, and C. N. R. Rao, Phys. Rev. B **54**, 15303 (1996).

[8] H. Kawano, R. Kajimoto, H. Yoshizawa, Y. Tomioka, H. Kuwahara, and Y. Tokura, Phys. Rev. Lett. **78**, 4253 (1997).

[9] P. Schiffer, A. P. Ramirez, W. Bao, and S. W. Cheong, Phys. Rev. Lett. **75**, 3336 (1995).

[10] H. Kuwahara, Y. Tomioka, A. Asamitsu, Y. Moritomo, and Y. Tokura, Science **270**, 961 (1995).

[11] D. P. Kozlenko, Z. Jirak, I. N. Goncharenko, and B. N. Savenko, J. Phys.: Condens. Matter **16**, 5883 (2004).

[12] A. Asamitsu, Y. Tomioka, H. Kuwahara, and Y. Tokura, Nature (London) **388**, 50 (1997).

[13] Ayan Guha, Arindam Ghosh, A. K. Raychaudhuri, S. Parashar, A. R. Raju, and C. N. R. Rao, Appl. Phys. Lett. **75**, 3381 (1999).

[14] L. Sudheendra, H. D. Chinh, A. R. Raju, A. K. Raychaudhuri, and C. N. R. Rao, Solid State Commun. **122**, 53 (2002).

[15] S. S. Rao, S. Tripathi, D. Pandey, and S. V. Bhat, Phys. Rev. B **74**, 144416 (2006).

[16] A. Biswas, I. Das, and C. Majumdar, J. Appl. Phys. **98**, 124310 (2005).

[17] Tapati Sarkar, A. K. Raychaudhuri, and Tapan Chatterji, Appl. Phys. Lett. **92**, 123104 (2008).

[18] K. Shantha Shankar and A. K. Raychaudhuri, J. Mater. Res. **21**, 27 (2006).

[19] Sigma-Aldrich, Inc. 3050 Spruce Street, St. Louis, MO 63103, USA.

[20] G. K. Williamson and W. H. Hall, Acta Metall. **1**, 22 (1953).

[21] MPMS SQUID Magnetometer, 6325 Lusk Boulevard, San Diego, CA 92121-3733, USA.

[22] Cryomech, Model PT405 Cryogenic Refrigerator, 113 Falso Drive, Syracuse, New York 13211 USA.

[23] http://www.ill.eu/sites/fullprof

[24] M. Dlouha, S. Vratislav, Z. Jirak, J. Hejtmanek, K. Knizek, and D. Sedmidubsky, Appl. Phys. A: Mater. Sci. Process. **74**, s673 (2002).

[25] Sohini Kar, Jayanta Sarkar, Barnali Ghosh, and A. K. Raychaudhuri, Phys. Rev. B **74**, 085412 (2006).

[26] Mandar A. Paranjape, K. Shantha Shankar, and A. K. Raychaudhuri, J. Phys. D **38**, 3674 (2005).

[27] Barnali Ghosh, Sohini Kar, Loveleen K. Brar, and A. K. Raychaudhuri, J. Appl. Phys. **98**, 094302 (2005).

[28] Z. H. Zhou, X. S. Gao, J. Wang, K. Fujihara, S. Ramakrishna, and V. Nagarajan, Appl. Phys. Lett. **90**, 052902 (2007).

[29] D. P. Kozlenko, L. S. Dubrovinsky, I. N. Goncharenko, B. N. Savenko, V. I. Voronin, E. A. Kiselev, and N. V. Proskurnina, Phys. Rev. B **75**, 104408 (2007).

[30] S. Rößler, U. K. Rößler, K. Nenkov, D. Eckert, S. M. Yusuf, K. Dorr, and K. H. Muller, Phys. Rev. B **70**, 104417 (2004).

[31] P. Kameli, H. Salamati, and A. Aezami, J. Appl. Phys. **100**, 053914 (2006).

[32] Ll. Balcells, B. Martinez, F. Sandiumenge, and J. Fontcuberta, J. Phys.: Condens. Matter **12**, 3013 (2000).